Amplitude Factorization Method in the Atmospheric Gravity-Wave Equation

Rein Rõõm[1] and Marko Zirk

Institute of Environmental Physics, Tartu University,

Ülikooli 18, Tartu 50090, Estonia

Abstract. A novel amplitude factorization method is applied to solve a discrete buoyancy wave equation with arbitrary wind and temperature height distribution. The solution is given in the form of a cumulative product of complex factors, which are computed by a nonlinear, inhomogeneous, two-member recurrence formula, initiated from a radiative condition on top. Singularities of the wave equation due to evanescent winds are eliminated by turbulent friction. The method provides an estimation of the minimal vertical resolution, required to attain a stable accurate solution. The areas of application of the developed numerical scheme are high resolution modelling of orographic waves for arbitrary orography in general atmospheric stratification conditions, and testing of adiabatic kernels of numerical weather prediction models.

Key words. Atmospheric gravity waves, linear buoyancy wave equation, arbitrary stratification, numerical solution, amplitude factorization method

[1]Correspondence to: Rein Rõõm, Institute of Environmental Physics, Tartu University. Ülikooli 18, Tartu 50090, Estonia E-mail: Rein.Room@ut.ee

1 Introduction

Models used for buoyancy wave studies can be divided into linear analytical [1 - 16] and nonlinear numerical (finite difference) schemes [17 - 31].

Advantages of the linear analytical approach are the high spatial and temporal resolution, a possibility to study stationary and transient regimes in separation, and the existence of analytical means for stability etc. analysis. The main disadvantage is the restriction to the simplest ('analytical') flow regimes (like the linear shear or constant stability).

Benefits of finite difference schemes lie in base-state generality, which supports realistic experimental conditions. Their main disadvantages are the moderate spatial resolution and inability to treat the steady and transient regimes separately.

In this paper, a novel method for the solution of the linear buoyancy wave equation is presented, combining the best of both approaches, being linear and (as much as possible) analytical, and at the same time numerical, accepting arbitrary vertical distributions of reference wind and temperature. The algorithm proves effective and fast, as it makes use of the direct computation of the attenuation factors of the wave amplitude via a straightforward recurrence formula with the initial value specification from a wave radiation condition on the top. The cumulative product of those factors from bottom to top yields a solution for the omega-velocity within a constant factor precision, the value of which is specified from bottom boundary condition.

Thus, solution of the wave equation will take very little effort and the major computational time goes to preparation of the equation coefficients and summation of the obtained orthogonal modes over wave numbers to get the solution in ordinary physical coordinates. Also, the numerical solution has a clear physical meaning, as the modulus of the complex attenuation factor presents the actual decrease of the wave amplitude per single layer of the discrete model, whereas its argument is the phase angle increment per layer.

As the model deals with variable winds, a problem arises inevitably with critical wave-vectors and critical levels, corresponding to singularities of the wave equation. This problem is solved in the current numerical approach with inclusion of turbulent friction in forcing terms, yielding singularity removal. The use of turbulent viscosity for wave-equation regularization was proposed already in [5,32,33]. However, the theoretical estimates of the maximum stable vertical grid-step will show that the requirements for high vertical resolution remain, especially in the vicinity of an evanescent wind level. This is the point where the numerical efficiency of the method becomes crucial, enabling the application of sufficiently high spatial resolution where appropriate.

While there exist various 'ready' wave equations they do differ rather substantially in appearance, depending on the 'small' details of the dynamical model, its coordinate system etc. To avoid potential ambiguities in basic definitions, we start with a short introduction of the wave equation used in this investigation from the Miller-Pearce-White (MPW) non-hydrostatic,

semi-elastic pressure-coordinate model [34, 35].

2 Buoyancy-wave equation

2.1. Continuous model

When using the non-dimensional log-pressure coordinate $\zeta = \ln(p_0/p)$, $\Rightarrow$ $p = p_0 \mathrm{e}^{-\zeta}$, ($p_0 = 1000\ hPa$ is the mean sea-level pressure) instead of the common pressure-coordinate p, the linearised stationary version of the MPW model reads

$$\mathbf{U} \cdot \nabla \omega = -R\frac{p}{H^2}T + \frac{p}{H^2}\frac{\partial \varphi}{\partial \zeta} + \gamma \nabla^2 \omega \ , \tag{1a}$$

$$\mathbf{U} \cdot \nabla \ \mathbf{v} = \mathbf{U}'\frac{\omega}{p} - \nabla \varphi - \mathbf{f} \times \mathbf{v} + \gamma \nabla^2 \mathbf{v} \ , \tag{1b}$$

$$\mathbf{U} \cdot \nabla \ T = \theta \frac{\omega}{p} + \gamma \nabla^2 T \ , \tag{1c}$$

$$\nabla \cdot \mathbf{v} - \frac{\partial \omega}{p \partial \zeta} = 0 \ . \tag{1d}$$

Horizontally, equations are written in the two-dimensional Cartesian system with the horizontal coordinates $\mathbf{x} = \{ \mathrm{x}, \mathrm{y}\}$; ∇ presents the horizontal gradient operator. Dynamic fields are the omega-velocity $\omega = dp/dt$ (with d/dt as material derivative), the temperature fluctuation T, the nonhydrostatic geopotential fluctuation φ, and the horizontal velocity fluctuation $\mathbf{v}$. The reference (background) state of the atmosphere is given by a stationary, horizontally homogeneous wind vector $\mathbf{U}(\zeta)$ with $\mathbf{U}' = \partial \mathbf{U}/\partial \zeta$, background

temperature $T^0(\zeta)$, gas constant for dry air R, and constant Coriolis parameter $f = |\mathbf{f}|$ where $\mathbf{f}$ is a vertical vector. The scale height H and the stability parameter θ are

$$H(\zeta) = \frac{RT^0(\zeta)}{g}, \qquad \theta(\zeta) = \frac{R}{c_p}T^0(\zeta) + \frac{\partial T^0}{\partial \zeta},$$

$\gamma = \gamma(\zeta)$ is the height-dependent kinematical turbulent viscosity coefficient.

Presenting dynamic fields as Fourier series

$$\{T, \omega, u, v, \varphi\} = \sum_{\mathbf{k}} \left\{ \hat{T}_{\mathbf{k}}, \hat{\omega}_{\mathbf{k}}, \hat{u}_{\mathbf{k}}, \hat{v}_{\mathbf{k}}, \hat{\varphi}_{\mathbf{k}}, \right\} \mathrm{e}^{\mathbf{i}\mathbf{k}\cdot\mathbf{x}},$$

where amplitudes $\hat{T}_{\mathbf{k}}, \hat{\omega}_{\mathbf{k}}, \hat{u}_{\mathbf{k}}, \hat{v}_{\mathbf{k}}, \hat{\varphi}_{\mathbf{k}}$ are functions of ζ, $\mathbf{i} = \sqrt{-1}$ is the imaginary unit and $\mathbf{k}$ is wave-vector, system (1) yields spectral amplitude equations

$$\mathbf{i}\nu\hat{\omega}_{\mathbf{k}} = -R\frac{p}{H^2}\hat{T}_{\mathbf{k}} + \frac{p}{H^2}\frac{\partial\hat{\varphi}_{\mathbf{k}}}{\partial\zeta} \ , \tag{2a}$$

$$\mathbf{i}\nu\hat{\mathbf{v}}_{\mathbf{k}} = \mathbf{U}'\frac{\hat{\omega}_{\mathbf{k}}}{p} - \mathbf{i}\mathbf{k}\hat{\varphi}_{\mathbf{k}} - \mathbf{f}\times\hat{\mathbf{v}}_{\mathbf{k}} \ , \tag{2b}$$

$$\mathbf{i}\nu\hat{T}_{\mathbf{k}} = \theta\frac{\hat{\omega}_{\mathbf{k}}}{p} \ , \tag{2c}$$

$$\mathbf{i}\mathbf{k}\cdot\hat{\mathbf{v}}_{\mathbf{k}} - \frac{\partial\hat{\omega}_{\mathbf{k}}}{p\partial\zeta} = 0 \ , \tag{2d}$$

where $\nu = \mathbf{U}(\zeta)\cdot\mathbf{k} + \mathbf{i}\gamma(\zeta)k^2$ is the intrinsic frequency or eigen-frequency. The eigen-frequency is complex in the presence of turbulent viscosity, which will produce weakening of the free orthogonal modes in time, or, in the case

of a stationary solution, down-stream and upward weakening of the wave amplitude in comparison with the inviscid case. From the linear system, after some algebra (see Appendix), a single second order equation results for the omega-velocity (short notation $\omega = \hat{\omega}_{\mathbf{k}}$ is used in the following)

$$\alpha \frac{\partial}{\partial \zeta} \frac{1}{\alpha} \frac{\partial \omega}{\partial \zeta} - \beta \frac{\partial \omega}{\partial \zeta} + \lambda \omega = 0, \tag{3}$$

with ζ-dependent coefficients

$$\alpha = \frac{p\nu}{\nu^2 - f^2}, \qquad \beta = \frac{\nu\rho + \mathbf{i}f\tau}{\nu^2 - f^2}, \qquad \lambda = k^2 H^2 \frac{N^2 - \nu^2}{\nu^2 - f^2} - \alpha \frac{\partial}{\partial \zeta} \frac{\nu\rho + \mathbf{i}f\tau}{p\nu}$$

$$\rho = \mathbf{k} \cdot \mathbf{U}', \qquad \tau = U_x' k_y - U_y' k_x, \qquad N^2 = \frac{R\theta}{H^2},$$

where N is the Brunt-Väisälä frequency. The lower and upper boundary conditions for this equation are the free slip condition on the bottom and evanescent omega velocity condition at the top

$$\omega(0) = \mathbf{ik}\cdot\mathbf{U}(0) p_{\mathbf{k}}(0), \qquad \lim_{\zeta \to \infty} \omega(\zeta) = 0. \tag{4}$$

In the case of uniform velocity $U_x', U_y' = 0, \quad \Rightarrow \quad \rho, \tau, \beta = 0, \ \nu = \text{const.}$, equation (3) simplifies to

$$\omega'' + \omega' + \lambda \omega = 0, \qquad \lambda = k^2 H^2 \frac{N^2 - \nu^2}{\nu^2 - f^2}. \tag{3'}$$

If, in addition, H, N are constants and the atmosphere is inviscid, $\gamma = 0$,

then λ is a real constant. In this particular case, the analytic solution of (3'), satisfying the upper boundary condition and the requirement of the wave group energy upward propagation (radiative condition, [36]), is

$$\omega = \begin{cases} \mathrm{e}^{-(1/2+\sqrt{1/4-\lambda}\,)\zeta}, \lambda < 1/4, \\ \mathrm{e}^{(-1/2+\mathbf{i}\sqrt{\lambda-1/4}\,)\zeta}, \lambda > 1/4. \end{cases} \tag{5}$$

If the non-homogeneous atmosphere is topped by a homogeneous inviscid layer, solution (5) holds there. We shall use this property to formulate the upper boundary condition for the discrete model.

2.2. Discretization

Let us introduce a staggered vertical grid with full levels ζ_j, and half levels $\zeta_{j+1/2}$,

$$0 = \zeta_{1/2} < \zeta_1 < .... < \zeta_{j-1} < \zeta_{j-1/2} < \zeta_j < \zeta_{j+1/2} < .... < \zeta_J < \zeta_{J+1/2} < \infty,$$

where J is the number of discrete layers. Layers are centred at ζ_j and layer boundaries are at levels $\zeta_{j\pm1/2}$. The discrete omega-velocity is located at half-levels: $\omega_{j+1/2}$, whereas differences are located at full levels:

$$\Delta\omega_j = \omega_{j+1/2} - \omega_{j-1/2}.$$

Auxiliary functions $\rho, \tau, \alpha, \beta, \lambda$ are defined for each ζ_j, and $\zeta_{j+1/2}$.

The discrete approximation of (3) is

$$L^+_{j+1/2}\Delta\omega_{j+1} - L^-_{j+1/2}\Delta\omega_j + \Delta\zeta^2_{j+1/2}\lambda_{j+1/2}\omega_{j+1/2} = 0, \tag{6}$$

with coefficients

$$L^+_{j+1/2} = \frac{\Delta\zeta_{j+1/2}}{\Delta\zeta_{j+1}}\left(\frac{\alpha_{j+1/2}}{\alpha_{j+1}} - \frac{1}{2}\Delta\zeta_{j+1/2}\beta_{j+1/2}\right),$$

$$L^-_{j+1/2} = \frac{\Delta\zeta_{j+1/2}}{\Delta\zeta_{j}}\left(\frac{\alpha_{j+1/2}}{\alpha_{j}} + \frac{1}{2}\Delta\zeta_{j+1/2}\beta_{j+1/2}\right).$$

where $\Delta\zeta_j = \zeta_{j+1/2} - \zeta_{j-1/2}$, $\Delta\zeta_{j+1/2} = \zeta_{j+1} - \zeta_j$. The bottom and top boundary conditions (4) become in the discrete case

$$\omega_{1/2} = \mathbf{ik}\cdot\mathbf{U}_{1/2}p_{\mathbf{k},1/2}, \qquad \lim_{\zeta_J\to\infty}\omega_{J+1/2} = 0. \tag{7}$$

The top condition here does not insist on exact zero at any finite top height $\zeta_{J+1/2}$, as this would cause spurious wave reflections on the top, but requires an asymptotic zero at $\zeta_{J+1/2} \to \infty$. The content of this condition will be described in more detail below.

3 Solution using factorization

Considering tentatively the jth layer homogeneous and inviscid, the solution in this layer is given by the exponential form (5), allowing to define the

attenuation factor of ω in the layer as

$$c_j \equiv \mathrm{e}^{\chi_j \Delta\zeta_j} = \frac{\omega_{j+1/2}}{\omega_{j-1/2}},$$

where χ_j is a complex phase shift in the layer of unit depth. The solution can be obtained on discrete half-levels as a cumulative product of attenuation factors

$$\omega_{j+1/2} = \omega_{1/2} \prod_{j'=1}^{j} c_{j'}, \qquad j = 1, 2, ...J, \tag{8}$$

with $\omega_{1/2}$, defined in (7). In the general non-homogeneous case, we will seek solution in the same form (8), though the layers are not homogeneous anymore (moreover, solution (8) does not need such a restrictive precondition but supports instead an assumption of continuous and differentiable profiles of the reference atmosphere inside layers). Inserting (8) into the wave equation (6) yields a two-point, nonlinear, non-homogeneous recurrence for c_j

$$L^{+}_{j+1/2}(c_{j+1} - 1) + L^{-}_{j+1/2}(1/c_j - 1) + \Delta\zeta^{2}_{j+1/2}\lambda_{j+1/2} = 0. \tag{9}$$

As it proves, the recurrence direction is an essential property here. Recurrence (9) is stable for a computation from top to bottom, in the direction of decreasing i and increasing ω, and it proves to be unstable in the opposite direction, if the top condition in (7) is applied, as ω is exponentially decreasing with height by absolute value. To apply recurrence (9), one has to know the top start value c_J. For this, it is advantageous to study first the

homogeneous sub-case.

3.1. Special case of homogeneous inviscid atmosphere

Homogeneous stratification in a discrete model assumes both a homogeneous background state and homogeneous layering

$$\mathbf{U} = \mathbf{const}., \qquad T^0, N = \text{const}., \qquad \Delta\zeta_j = \Delta\zeta_{j+1/2} = \Delta\zeta. \tag{10}$$

In this case $\beta_{j+1/2} = 0$, while $L^{\pm}$ and λ in (6) become height-independent

$$L^{\pm}_{j+1/2} = L^{\pm} = \mathrm{e}^{\pm\Delta\zeta/2}, \qquad \lambda_{j+1/2} = \lambda = H^2k^2\frac{N^2-\nu^2}{\nu^2-f^2}.$$

Considering the friction-free atmosphere, $\gamma = 0$, we will have $\nu = \mathbf{k}\cdot\mathbf{U}$, i.e., λ becomes a real constant. To the homogeneous continuous solution (5), in the discrete, homogeneous, friction-free model, index-independent attenuation factors correspond:

$$c_j = c, \tag{11}$$

resulting in the reduction of the general recurrence (9) to a quadratic equation for c, identical for each ith level:

$$\mathrm{e}^{\Delta\zeta/2}(c-1) + \mathrm{e}^{-\Delta\zeta/2}(c^{-1}-1) + (\Delta\zeta)^2\lambda = 0.$$

This quadratic equation has two solutions, from which only those, providing top condition (7) and corresponding to the radiative condition are shown

next. Solutions depend on the parameter

$$Q = \cosh(\Delta\zeta/2) - \frac{1}{2}(\Delta\zeta)^2\lambda. \tag{12}$$

There exist three regions: $Q \leq -1$, $-1 < Q < 1$, and $Q \geq 1$ with different behaviour of the solution. For $Q \leq -1$ a physically meaningful solution does not exist. This indicates that $\Delta\zeta$ was chosen too large and should be reduced, because $\lim_{\Delta\zeta\to 0} Q = 1$. The two other options describe the free and evanescent (or trapped, [36]) waves:

$$c = \begin{cases} \mathrm{e}^{\Delta\zeta(-1/2+\mathrm{i}\xi),} & -1 < Q < 1\ , \\ \mathrm{e}^{-\Delta\zeta(1/2+q),} & Q > 1\ , \end{cases} \tag{13}$$

where

$$q = \frac{\ln\left(Q + \sqrt{Q^2-1}\right)}{\Delta\zeta}, \qquad \xi = \frac{1}{\Delta\zeta} \cdot \begin{cases} \arctan\frac{\sqrt{1-Q^2}}{Q}, & Q > 0, \\ \pi/2, & Q = 0\ , \\ \pi - \arctan\frac{\sqrt{1-Q^2}}{|Q|}, & Q < 0\ . \end{cases} \tag{14}$$

The discrete solution (8) becomes in terms of attenuation factor (13)

$$\omega_{j+1/2} = \omega_{1/2} \cdot \begin{cases} \mathrm{e}^{j\Delta\zeta(-1/2+\mathrm{i}\xi),} & -1 < Q < 1\ , \\ \mathrm{e}^{-j\Delta\zeta(1/2+q),} & Q > 1\ , \end{cases} \tag{15}$$

which presents the discrete approximation to the exact solution (5). If

$$\Delta\zeta << 1, \tag{16}$$

which corresponds to the vertically high-resolution case, then

$$Q \approx 1 + \frac{\Delta\zeta^2}{2}\left(\frac{1}{4} - \lambda\right).$$

If, in addition,

$$\left|\frac{\Delta\zeta^2}{2}\left(\frac{1}{4} - \lambda\right)\right| << 1, \tag{17}$$

then $q \to \sqrt{1/4 - \lambda}$, $\xi \to \sqrt{\lambda - 1/4}$, and the discrete approximation (15) will approach the exact solution (5).

Due to exponential decay of solution (15) with height, the top boundary condition (7) holds, indeed.

3.2. Recurrence initialization in non-homogenous case

We can always assume that there is a homogeneous inviscid layer at the top, with stratification parameters corresponding to the topmost discrete layer with index $j = J$:

$$\Delta\zeta = \Delta\zeta_J, \quad \mathbf{U} = \mathbf{U}_J, \quad T^0 = T^0_J \quad \to \quad \lambda = \lambda_{\mathbf{k},J}.$$

The starting value c_J in recurrence (9) can be chosen then as the attenuation factor of this homogeneous top layer

$$c_J = c \quad \text{from (13), (14)} .$$

3.3. Requirements of vertical resolution

In the high vertical resolution case (16), the attenuation factors c_j are supposed to be, and $L^{\pm}$ are, close to unity in absolute terms, yielding a constraint to the free term in (9)

$$\Delta\zeta_{j+1/2}^2 \left|\lambda_{j+1/2}\right| << 1 \tag{18}$$

(rather close to condition (17)). In the case of an inviscid atmosphere, $\lambda_{j+1/2}$ can become infinite for critical wave-vectors $\mathbf{k}^*$ (specific for each level j), for which $\nu_j^2 - f^2 = (\mathbf{k}^* \cdot \mathbf{U}_j)^2 - f^2 = 0$, yielding $\Delta\zeta_{j+1/2} \to 0$ in (18). Due to discrete nature, the wave-vectors are not (except in the case of the special choice of $\mathbf{U}_j$) strictly critical, but a lot of them can be nearly critical, $(\mathbf{k}^* \cdot \mathbf{U}_j)^2 - f^2 \approx 0$, which would cause very large λ and unfeasibly small $\Delta\zeta$. Especially important for the numerical solution accuracy are levels with evanescent wind $\mathbf{U} \to 0$, as the corresponding critical wave-vectors are located in the maximum area of spectral amplitudes. The closest neighbourhood of the evanescent wind level is therefore called the critical layer. As numerical experimentation shows, a critical layer forms if $|\mathbf{U}_j| < 1$ to 1.5 m/s . In the case of an inviscid atmosphere, it is impossible to satisfy (18) for any computationally usable size of $\Delta\zeta$ in the critical layer. Fortunately, the introduction of a rather moderate turbulent friction will regularize λ, as $\nu_j^2 - f^2 = (\mathbf{k} \cdot \mathbf{U}_j + \mathbf{i}\gamma k^2)^2 - f^2$ can't become zero anywhere.

Using in the vicinity of critical wave-vectors an approximation $\lambda \sim k^2 H^2 N^2/(\nu^2 -$

f^2), (18) gives

$$\Delta\zeta_{j+1/2} < \frac{1}{\sqrt{|\lambda_{j+1/2}|}} \approx \frac{\sqrt{|\nu^2_{j+1/2} - f^2|}}{kH_{j+1/2}N_{j+1/2}}.$$

As $\sqrt{|\nu^2_{j+1/2} - f^2|} = \left\{\left[(\mathbf{k}\cdot\mathbf{U})^2 + \gamma^2k^4 - f^2\right]^2 + 4\gamma^2f^2k^4\right\}^{1/4}_{k+1/2} \geq k\sqrt{2\gamma_{j+1/2}f}$, a suitable estimation of the maximum vertical grid-step is

$$\Delta\zeta_{j+1/2} < \frac{\sqrt{2f\gamma_{j+1/2}}}{H_{j+1/2}N_{j+1/2}}. \tag{19}$$

Being independent of the horizontal wave-vector $\mathbf{k}$, this condition presents a 'global' estimate, enabling an accurate solution for all horizontal spectral modes. It is convenient to present the diffusion coefficient as

$$\gamma_{j+1/2} = \gamma^0_{j+1/2}N_{j+1/2}\Delta x^2/2 \tag{20}$$

The nondimensional parameter $\gamma^0_{j+1/2}$ has a simple meaning: $1/\gamma^0_{j+1/2}$ is the e-folding decrease period in units $1/N$ of the highest horizontally resolved gravity wave mode with scale $\sim \Delta x$. In the discrete case, Δx is the horizontal grid-length; in the horizontally continuous formalism, Δx can be estimated as the internal spatial scale of orography. From (19) and (20) we get finally

$$\Delta\zeta_{j+1/2} < \frac{\Delta x}{H_{j+1/2}}\sqrt{\gamma^0_{j+1/2}f/N_{j+1/2}}. \tag{21}$$

As an example, $\Delta z = H\Delta\zeta < 10$ m for $\Delta x = 1$ km, $\gamma^0 = 10^{-2}$, $f/N =$

10^{-2}. This vertical resolution limit decreases to 1 m for a ten times higher horizontal resolution $\Delta x = 100$ m.

Condition (21) should not be interpreted as an exact upper limit, but rather as a rough estimation of the vertical resolution, that is expected to provide the required solution accuracy. However, as numerical experimentation shows, (21) provides faithful estimates in all instances.

4 Examples

In the following examples, a horizontally discrete Fourier transform is applied to orography, which corresponds to the 'witch of Agnesi' profile

$$h(x,y) = \frac{h_0}{[1 + (x - x_0)^2/a_x^2 + (y - y_0)^2/a_y^2]^{3/2}},$$

where the maximum height h_0, central coordinates x_0, y_y, and half-widths in the directions of coordinate axes a_x, a_y are constant parameters. The spectral wave equation is solved using the above-described solution factorization approach, and the result is then inverted back to physical space. Vertical velocity w = - $H\omega/p$ is shown in all examples.

Figure 1 presents the wave pattern of w for one-dimensional Agnesi ridge with $h_0 = 100$ m, $a_x = 2$ km, $a_y = \infty$. Reference temperature $T^0(p)$ presents a climatological profile (280 K on surface, lapse rate 6.5 K/km in the troposphere, and constant 202 K in the stratosphere). The unidirectional wind equals U_x

= 12 m/s at the surface, has a shear of 0.25 m/s/km in the troposphere, and becomes constant $U_x = 15$ m/s in the stratosphere. The tropopause height is 12 km. Horizontal resolution is $\Delta x = 500$ m, grid-domain in the x-direction is 2048 points. Vertical resolution is chosen to be $\Delta z = 100$ m, ($\Delta\zeta \approx 0.01$), and $J = 300$ levels, while the atmosphere is inviscid with $\gamma^0 = 0$ at all levels. Experiments show, that an increase in vertical resolution and the introduction of a weak ($\gamma^0 = 0.01$) viscosity do not alter modelling results. However, stronger friction with $\gamma^0 = 0.05$ would damp the wave-field moderately.

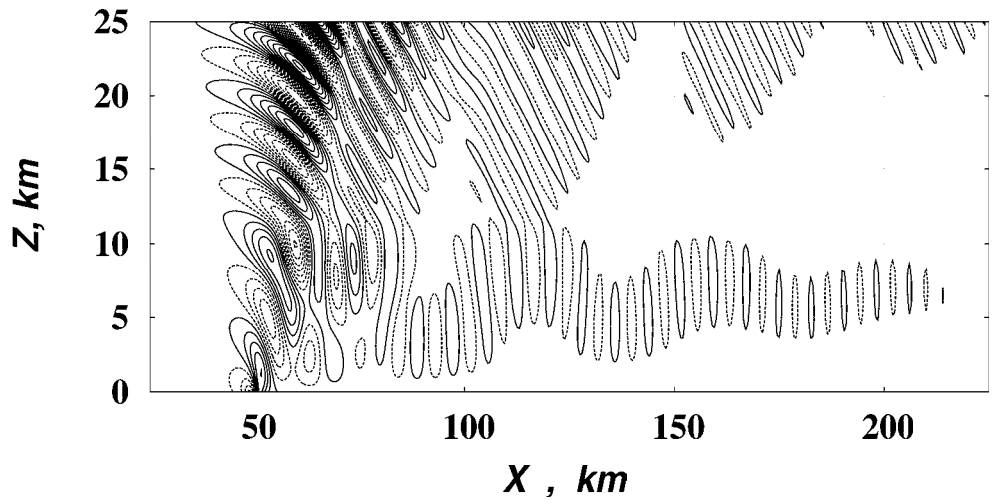

Fig. 1. Tropospheric wave-guide formation due to the combined effect of the tropopause and wind shear. Vertical velocity contours with a $\Delta w = 0.1\ ms^{-1}$ interval are shown.

While the buoyancy wave reflection at the tropopause and the tropospheric wave-guide formation has been theoretically proven some time ago [37] there

have been little numerical experimentation showing the details of the process. As seen in Fig. 1. even a rather moderate tropospheric wind shear may cause substantial wave reflection at the tropopause and generation of wave trains. The wave train increases in length with the wind shear intensification and can reach several thousands kilometres (depending on the intensity of turbulent friction). The current example has special interest due to the wave-train wiggling, which is observable at weak shear and would disappear with shear strengthening.

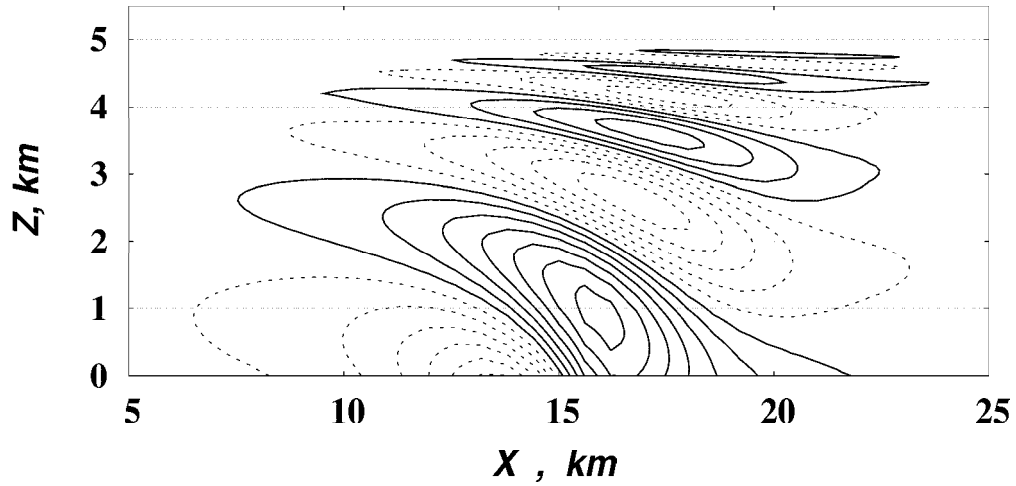

Fig. 2. Wave absorption at the critical layer, located near $z = 5$ km. Vertical velocity contours with $\Delta w = 0.05\ ms^{-1}$ interval are shown.

Fig. 2. presents a flow over an Agnesi ridge with $h_0 = 100$ m, $a_x = 3$ km, $a_y = \infty$ and with the same temperature profile as in the previous case. However, the wind is backing with height in this model, having a value 10 ms^{-1} at the surface and decreasing linearly with height. It becomes zero at the 5

km level, which defines the central height of the respective critical layer, and decreases with height further to a constant value -2.0 ms^{-1} at the 5.5 km height, approximately.

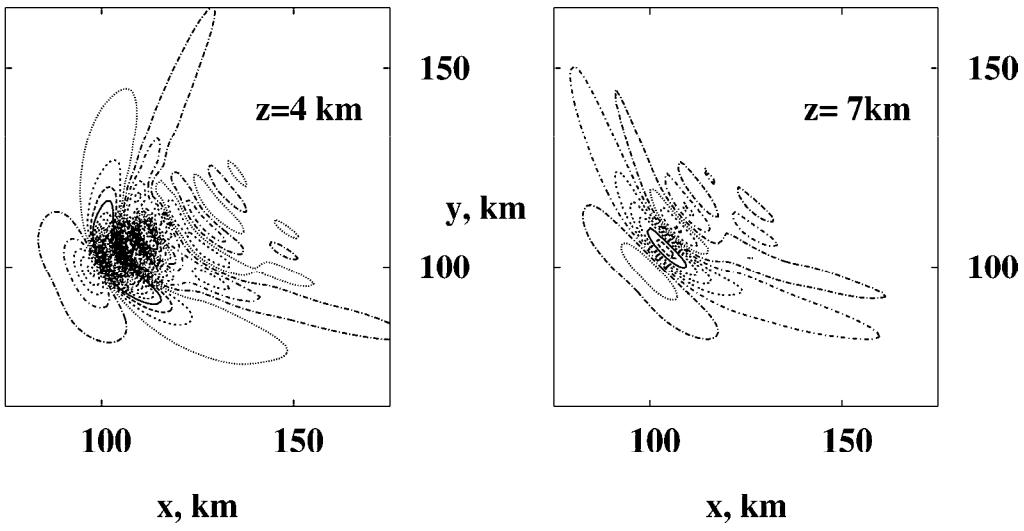

Fig. 3. Horizontal cross-section of the vertical velocity at different heights over a circular hill. The main flow is sheared both in speed and direction. Isotachs are drawn with a 0.2 m/s interval.

Horizontal resolution is 500 m and the number of horizontal grid-points is 256. Vertical grid-step decreases linearly with height from $\Delta z = 100$ m at the surface to $\Delta z = 5$ m at the wind reversal level, above which it is kept constant. The number of vertical levels is 240, turbulent viscosity $\gamma^0 = 0.05$. The main aim of this example is to demonstrate the need of enhanced resolution in the vicinity of the critical layer. The coincidence with earlier

reported results [28, 38 - 40] is excellent, demonstrating complete absorption of orographic buoyancy waves at the critical layer.

Fig. 3. shows horizontal cross-sections of w at different heights for a wind sheared both in amplitude and direction, blowing over a circular hill with $h_0 = 300$ m, $a_x = a_y = 3$ km. Horizontal resolution is $\Delta x = \Delta_y = 1.1$ km, the horizontal grid consists of 256x256 points. The model has 300 levels with constant resolution $\Delta z = 50$ m in the vertical. The turbulent viscosity $\gamma^0 = 0.05$. The reference atmosphere is isothermal with $T^0 = 280$ K. The wind amplitude is a hyperbolic function of height with maximum of 40 m/s at $z = 15$ km, while wind direction rotates uniformly with height:

$$u_x = U(z)cos(\pi z/z_{rev}), \qquad u_y = U(z)sin(\pi z/z_{rev}), \qquad z_{rev} = 12km,$$

$$U(z) = U_s + U_0 \left(1 - \frac{z}{z_{Jax}}\right) \frac{z}{z_{Jax}}, \quad U_s = 10m/s, \; U_0 = 120m/s, \; z_{Jax} = 30km.$$

The solution is fond to be insensitive to vertical resolution doubling, which means that a constant resolution $\Delta z = 50$ m is sufficient here. However, the decrease of γ^0 to 0.01 implies a need of a vertical grid-step decrease to $\Delta z = 20$ m.

The qualitative coincidence of the present example with former analytical [41] and numerical [38] results is excellent, although a quantitative comparison is not available in the analytical case, as models with such a wind complexity are not solved analytically yet. The typical feature of this kind of flow regimes with uniform directional wind shear is the complete buoyancy wave

absorption at the wind reversal height.

5 Conclusions

The described method presents a simple and fast orographic wave modelling tool in the case of rather sophisticated flow regimes both in two- and three dimensional cases. Experiments with realistic height-dependent temperature, including the tropopause, and optional sheared winds, are attainable. Rather large modelling domains in association with high horizontal and vertical resolutions can be used, making high-resolution modelling of extended wave-fields possible. As an example, in a two-dimensional case, with a horizontal domain of 5000 km length and a 500 m horizontal resolution, and 1000 levels in vertical with 10 m vertical resolution, would require $\sim$ 1 minute computation in a PC.

Compliance with the vertical resolution condition (21) is really essential in conditions with an evanescent wind. In that case, very high vertical resolutions are required near and at the critical layer, located around the zero-wind level (up to $\Delta z \sim 1$ m for horizontal resolutions $\Delta x \sim 100$ m).

However, for relatively large reference winds (U = 10 m/s can already be considered as 'large'), condition (21) can be weakened. For example, at horizontal resolutions $\Delta z \geq 1$ km, vertical resolution $\Delta z = 100$ m can be considered sufficient in most cases.

The area of application of the proposed numerical solution is high resolu-

tion modelling of orographic waves for arbitrary orography in complex atmospheric stratification conditions. The model can be applied also as a test-tool for checking numerical accuracy of adiabatic kernels of the nonlinear nonhydrostatic NWP models.

Acknowledgments

Authors are grateful to Per Unden and Pedro M. Miranda for fruitful discussion of the subject and proposing of many valuable corrections to the manuscript.

This investigation has been supported by Estonian Science Foundation under Research Grant 5711.

Appendix

Wave equation derivation

Equations for divergence $D = \mathbf{i}\mathbf{k} \cdot \hat{\mathbf{v}}_\mathbf{k}$ and vorticity $\zeta = \mathbf{i}(k_x\hat{v}_y - k_y\hat{v}_x)$ from (2b) are:

$$\mathbf{i}\nu D = \mathbf{i}\frac{\rho}{p}\hat{\omega}_k + k^2\hat{\varphi}_k + f\zeta, \qquad \mathbf{i}\nu\zeta = -\mathbf{i}\frac{\tau}{p}\hat{\omega} - fD.$$

Ellimination of ζ from these realtionships with subsequent substitution of D from (2d) yields

$$\frac{1}{\alpha}\frac{\partial\hat{\omega}_k}{\partial\zeta} - \left(\rho + \mathbf{i}\frac{f}{\nu}\tau\right)\frac{\hat{\omega}_k}{p} = -\mathbf{i}\mu^2\hat{\varphi}_k. \qquad (A1)$$

Another relationship between φ and ω follows from (2a), (2c):

$$H^2 \frac{\nu^2 - N^2}{\nu} \hat{\omega}_k = -\mathbf{i} \frac{\partial \hat{\varphi}}{\partial \zeta}. \qquad (A2)$$

Elimination of φ from (A1) and (A2) gives equation (3).

References

[1] P. Queney, The problem of airflow over mountains. A summary of theoretical studies, Bull. Amer. Met. Soc. 29 (1948) 16 – 26.

[2] R. S. Scorer, Theory of waves in the lee of mountains, Q. J. R. Meteorol. Soc. 75 (1949) 41 – 56.

[3] M. G. Wurtele, The three-dimensional lee wave. Beitr. Phys. Atmos. 29 (1957) 242 - 252.

[4] G. D. Crapper, A three-dimensional solution for waves in the lee of mountains, J. Fluid Mech. 6 (1959) 51 -76.

[5] W. L. Jones, Propagation of internal gravity waves in fluids with shear flow and rotation, J. Fluid Mech. 30 (1967) 439 - 488.

[6] R. B. Smith, Linear theory of stratified hydrostatic flows past an isolated mountain, Tellus 32 (1980) 348 - 364.

[7] G. S. Janovich, Lee waves in three-dimensional stratified flow, J. Fluid Mech. 148 (1984) 97 - 108.

[8] R. D. Sharman, M. G. Wurtele, Ship waves and lee waves, J. Atmos. Sci.

75 (1983) 41 - 56.

[9] A. S. Broad, Linear theory of momentum fluxes in 3-D flows with the turning of the mean wind with height Q. J. R. Meteorol. Soc. 121 (1995) 1891 - 1902.

[10] J.-P. Pinty, R. Benoit, E. Richard, R. Laprise, Simple tests of a semi–implicit semi–Lagrangian model on 2D mountain wave problems, Mon. Weather Rev., 123 (1995) 3042 – 3058.

[11] G. J. Shutts, Gravity-wave drag paramterization over complex terrain. The effect of critical level absorption in directional wind shear, Q. J. R. Meteorol. Soc. 121 (1995) 1005 - 1021.

[12] R. Rõõm, A. Männik, Response of different nonhydrostatic, pressure-coordinate models to orographic forcing. J. Atmos. Sci. 56 (1999) 2553 – 2578.

[13] W. T. Welch, P. Smolarkiewitz, The large-scale effects of flow over periodic mesoscale topography, J. Atmos. Sci. 58 (2001) 1477 - 1492.

[14] D. Broutman, J. W. Rottman, S. D. Eckermann, A simplified Fourier method for nonhydrostatic mountain waves, J. Atmos. Sci. 60 (2003) 2686 - 2696.

[15] A. Männik, R. Rõõm, A. Luhamaa, Nonhydrostatic generalization of a pressure-coordinate-based hydrostatic model with implementation in HIRLAM: validation of adiabatic core, Tellus 55A (2003) 219 – 231.

[16] L. M. Polvani, R. K. Scott, S. J. Thomas, Numerically converged solu-

tions of the global primitive equations for testing the dynamical core of atmospheric GCMs, Mon. Weather Rev., 132 (2004) 2539 - 2552.

[17] R. R. Long, Some aspects of the flow of stratified fluids. Part I: A theoretical investigation, Tellus 5 (1953) 42 – 58.

[18] P. G. Drazin, D. W. Moore, Steady two-dimensional flow of fluid of variable density over an obstacle, J. Fluid Mech. 28 (1967) 353 – 370.

[19] J. W. Miles, Lee waves in a stratified flow. Part 1. Thin barrier, J. Fluid Mech. 32 (1968) 549 - 567.

[20] T. L. Clark, A small–scale dynamic model using a terrain following coordinate transformation, J. Comput. Phys. 24 (1977) 186 – 215.

[21] J. B. Klemp, D. K. Lilly, Numerical simulation of hydrostatic mountain waves, J. Atmos. Sci. 35 (1978) 78 – 107.

[22] D. R. Durran, J. B. Klemp, A compressible model for the simulation of moist mountain waves, Mon. Weather Rev., 111 (1983) 2341 – 2361.

[23] R. Laprise, W. R. Peltier, On the structural characteristics of steady finite–amplitude mountain waves over bell–shaped topography, J. Atmos. Sci. 46 (1989) 586 – 595.

[24] M. G. Wurtele, R. D. Sharman, T. L. Keller, Analysis and simulations of a troposphere-stratosphere gravity wave model. Part I, J. Atmos. Sci. 44 (1987) 3269 – 3281.

[25] M. Xue, A. J. Thorpe, A mesoscale numerical model using the nonhydrostatic pressure-based sigma-coordinate equations. Model experiments

with dry mountain flows, Month. Wea. Rev. 119 (1991) 1168 – 1185.

[26] P. M. A. Miranda, I. N. James, Non-linear three-dimensional effects on gravity-wave drag. Splitting flow and breaking waves, Q. J. R. Meteorol. Soc. 118 (1992) 1057 – 1081.

[27] J. W. Rottman, D. Broutman, R. Grimshaw, Numerical simulation of Uniformly stratified flow over topography, J. Fluid Mech. 306(1996) 1 - 30.

[28] P. M. A. Miranda, M. A. Valente, Critical level resonance in tree–dimensional flow past isolated mountains, J. Atmos. Sci. 54 (1997) 1574 – 1588.

[29] L. B. Nance, D. R. Durran, A modeling study of nonstationary trapped mountain lee waves. Part I. Mean-flow variability, J. Atmos. Sci. 55 (1997) 2275 – 2291.

[30] R. Rõõm, P. M. A. Miranda, A. J. Thorpe, Filtered non-hydrostatic models in pressure-related coordinates, Q. J. R. Meteorol. Soc. 127 (2001) 1277-1292.

[31] M. A. C. Teixeira, P. M. A. Miranda, The effect of wind shear and curvature on the gravity wave drag, J. Atmos. Sci. 61 (2004) 2638 – 2643.

[32] C. C. Lin, *The Theory of Hydrodynamic Instability.* Cambridge: Cambridge Univ. Press. (1955)

[33] P. Hazel, The effect of viscosity and heat conduction on internal gravity

waves at a critical level, J. Fluid Mech. 30 (1967) 775 - 783.

[34] M. J. Miller, R. P. Pearce, A three-dimensional primitive equation model of cumulonimbus convection, Q. J. R. Meteorol. Soc. 100 (1974) 133 – 154.

[35] A. A. White, An extended version of nonhydrostatic, pressure coordinate model, Q. J. R. Meteorol. Soc. 115 (1989) 1243 – 1251.

[36] P. G. Baines, *Topographic Effects in Stratified Flows.* Cambridge Univ. Press (1995) 482 pp.

[37] A. Eliassen, On the meso-scale mountain waves on the rotating Earth, Geofys. Publicasjoner 27 (1968) 1 - 15.

[38] V. Grubiŝić, P. K. Smolarkiewicz, The effect of critical levels on 3D orographic flows. Linear regime, J. Atmos. Sci. 54 (1997) 1943 - 1960.

[39] Bo-Wen Shen, Yuh-Lang Lin, Effects of critical levels on two-dimensional back-sheared flow over an isolated mountain ridge, J. Atmos. Sci. 56 (1999) 3286 - 3302.

[40] G. J. Shutts, A. Gadian, Numerical simulations of orographic gravity waves in flows which back with height, Q. J. R. Meteorol. Soc. 125 (1999) 2743 - 2765.

[41] G. J. Shutts, Inertia-gravity wave and neutral Eady wave trains forced by directionally sheared flow over isolated hills, J. Atmos. Sci. 60 (2003) 593 - 606.

Figure captions

Fig. 1. Tropospheric wave-guide formation due to the combined effect of the tropopause and wind shear. Vertical velocity contours with a $\Delta w = 0.1$ ms^{-1} interval are shown.

Fig. 2. Wave absorption at the critical layer, located near $z = 5$ km. Vertical velocity contours with $\Delta w = 0.05$ ms^{-1} interval are shown.

Fig. 3. Horizontal cross-section of the vertical velocity at different heights over a circular hill. The main flow is sheared both in speed and direction. Isotachs are drawn with a 0.2 m/s interval.